

Article

# PIV Experimental Research and Numerical Simulation of the Pigging Process

Shengtao Chen <sup>1,2,\*</sup>, Yuhan Zhang <sup>1</sup>, Tianyu Su <sup>1</sup> and Yongjun Gong <sup>1,2</sup>

<sup>1</sup> College of Naval Architecture and Ocean Engineering, Dalian Maritime University, Dalian 116026, China; a1759213574@163.com (Y.Z.); subb1003@163.com (T.S.); gyj@dlnu.edu.cn (Y.G.)

<sup>2</sup> Liaoning Provincial Key Laboratory of Rescue and Salvage Engineering, Dalian Maritime University, Dalian 116026, China

\* Correspondence: dmucst@dlnu.edu.cn

**Abstract:** The initial running speed of the pig during gas–liquid two-phase pipeline pigging can significantly influence the velocities of both gas and liquid phases within the pipeline. However, due to the complexity and limited understanding of these velocity variations, developing an effective operational plan for pigging becomes challenging. To enhance pigging efficiency and effectively seal the pig, it is crucial to monitor the velocity variations in the gas–liquid phase within the pipeline. In this study, an experimental platform was established to facilitate precise observation of these variations. Particle image velocimetry (PIV) technology was employed for a comprehensive understanding of gas–liquid two-phase velocities during pig operation in the pipeline. The experimental results demonstrated that increasing both the velocity and the initial liquid level height of the pig resulted in a corresponding augmentation of velocity fluctuation range. Specifically, at a holdup rate of 30%, there was a 10% reduction in the maximum liquid-phase velocity, while at a holdup rate of 25%, this reduction amounted to 16% compared to the pigging velocity.

**Keywords:** gas–liquid two-phase; PIV test; PIG; numerical simulation



**Citation:** Chen, S.; Zhang, Y.; Su, T.; Gong, Y. PIV Experimental Research and Numerical Simulation of the Pigging Process. *J. Mar. Sci. Eng.* **2024**, *12*, 549. <https://doi.org/10.3390/jmse12040549>

Academic Editor: Dejan Brkić

Received: 16 February 2024

Revised: 11 March 2024

Accepted: 20 March 2024

Published: 25 March 2024



**Copyright:** © 2024 by the authors. Licensee MDPI, Basel, Switzerland. This article is an open access article distributed under the terms and conditions of the Creative Commons Attribution (CC BY) license (<https://creativecommons.org/licenses/by/4.0/>).

## 1. Introduction

The transportation of oil and natural gas through industrial pipelines has seen a growing prevalence of gas–liquid two-phase flow [1]. Over time, these pipelines may encounter issues such as leaks, blockages, and corrosion within their walls. Therefore, it is imperative to regularly monitor and clean the pipeline [2]. Currently, pipeline robots are capable of pigging operations and surveillance. Different working principles exist for pipeline systems; some rely on water flow and pressure while others are controlled by electricity [3]. In the case of gas–liquid two-phase flow, changes in the flow field structure occur, making it unclear how the pipeline robot generates flow velocity during operation. Consequently, there may be difficulties in selecting appropriate settings for different working conditions which can hinder the intended prolongation of its operational lifespan. Additionally, due to uncertain fluctuations in gas–liquid-phase velocity during long-term pigging operations, accurately determining pipeline corrosion becomes challenging thereby impeding the provision of an effective anti-corrosion program for the pipeline. Figure 1 illustrates examples of corrosion inside the pipeline.

The determination of liquid-phase fluctuations within the pipeline remains a crucial task for Hudaya et al. [4]. In their study, a high-speed camera employed to capture and analyze the variations in the liquid level within a pipeline with an inner diameter of 26 mm. Revised sentence: “Subsequently, an experimental analysis was conducted on the fluctuation characteristics of air–water laminar flow using advanced image processing technology, yielding valuable insights into the variations in gas and liquid surface velocities. A two-fluid model was employed by Figueiredo et al. [5] to numerically simulate the stratified two-phase flow in a natural gas pipeline. The two-fluid model is based on the momentum

and continuity equations within the average control volume, considering solid particles as continuous phases. Assuming the compressibility of the gas phase and incompressibility of the liquid phase, a constant temperature is maintained throughout the flow. The successful determination of the hyperbolic nature of this two-fluid model (i.e., different characteristic roots are obtained during solving). The findings are consistent with the flow outcomes observed in offshore gas pipelines. Previous studies have been conducted to determine the velocity of both gas and liquid phases in pipelines, considering their initial conditions. Xu, X and colleagues [6] specifically investigated the condensation phenomenon occurring within natural gas transmission pipelines. Numerical simulation was employed to model pig tracking and slug length increase during pipeline robot pigging operations, demonstrating high computational accuracy suitable for engineering design applications." Sadeghi et al. [7] investigated the impact of Pipeline Inspection Gauge (PIG) parameters on the dynamic response of surface pipelines during pigging operations. Previous studies have demonstrated that the physical characteristics of PIGs play a pivotal role in determining the dynamics of pipeline systems. In their study, Wen et al. [8] developed a model for pigging pipelines that incorporates stress and vibration equations. The research conducted by Liu, Y and colleagues [9] provides valuable assistance in the technical and theoretical aspects of pigging operations. Their analysis focused on the impact of varying inlet mass flow rate and pig shitter ratio on critical parameters such as bottom pressure of the lift pipe, pig velocity, and liquid-phase distribution pattern. The findings indicate that employing a bypass pig during severe slug flow conditions can significantly reduce pressure fluctuations at the bottom of the riser compared to using a conventional pig, as well as decrease pig speed. Deng et al.'s study [10] examined pressure drop characteristics in gas-liquid flow through T-shaped steep slopes and curved drainage pipes. The findings can be utilized for pig tracking and hydraulic pulse prediction, enabling determination of the pig's position and speed. Given the current state of pig development, wax removal by pigs is inadequate, and the mechanism for wax removal remains to be elucidated. Wang et al. [11] conducted experiments on wax removal using various models of non-super-diameter polyurethane pigs. Their findings are pivotal in determining the optimal dewaxing frequency and assessing associated risks with pig usage. Nieckele et al. [12] performed simulations to study the movement of a pig through a pipeline containing gas and liquid phases. A stick-slip model was employed to simulate the contact force between the pig and pipe wall, while finite element analysis predicted the contact force between a disc-shaped pig and pipe wall. Mirshamsi et al. [13] conducted a dynamic analysis and simulation of a long pig traversing a two-dimensional gas pipeline, demonstrating that the established equation enables real-time estimation of the pig's position and velocity. Sousa et al. [14] proposed an indirect predictive maintenance method for systematic evaluation of internal pipe sections, providing a valuable contribution to the existing knowledge base. By utilizing continuous field measurements, it becomes possible to predict pigging times and prevent severe clogging. Hendrix et al. [15] conducted experimental and numerical investigations on bypass pigging under low-pressure conditions, making significant contributions to the design of pipeline inspection meters. The presence of a bypass hole in the pig reduces its speed, leading to uneven movement and an increased risk of pig sticking. To address this issue, Li et al. [16] developed a transient steady-state analysis model for studying the uneven movement of pigs and subsequently proposed a shutdown model for pigs. The experimental data obtained were found to be consistent with the simulated speed trend, thereby validating the accuracy of their analytical model. Jamshidi et al. [17] developed a simplified pigging model for a two-phase flow pipeline with a diameter of 657 mm and a sea line length of 108 km in the South Pars region of southern Iran to predict pigging operations. This model was developed in conjunction with engineering practice. The numerical simulation results are compared to three pigging displacements, which agree. To accurately detect the speed of a pig during bypass, Chen et al. [18] suggested using an infrared ray-based method. The experimental results indicate that the bypass pig's average velocity changes linearly with the driving gas flow. In contrast, the velocity difference of

the gas pig remains constant at the same bypass fraction. Zhang et al. [19] analyzed gas backflow in the bypass valve and pipeline during the operation process of the pig in a hilly gas transmission pipeline. The study reveals that gas velocity significantly impacts bypass pig speed, followed by bypass area and friction force. Wu et al. [20] conducted an experimental study on the pigging process at natural gas pipeline aerial crossings, including simulation and dynamic response. Due to the lack of empirical research, the main problem is the fluid–structure coupling vibration caused by two phases for more complex structures. Based on current research, gas–liquid two-phase flow in pipelines is well established in numerical simulation. To ensure the accuracy and practicality of research findings, it is imperative to conduct experiments to understand the actual patterns of gas and liquid-phase velocity changes [21]. However, we encountered several challenges during these experiments, including the frequent occlusion of the pig during prolonged operation. A study conducted by Yelgaonkar et al. [22] utilized radioisotope technology to locate pipeline blockages caused by pigs. The team could accurately determine the block's location using radioactive tracer technology, such as gamma scanning and radiography. Another study by Zhang et al. [23] aimed to test the reliability of PIV experimental results in rectangular micro pipelines. The team used micro-PIV to measure the flow under three working conditions with Reynolds numbers 47, 127, and 215, respectively. Their results agreed with the theoretical velocity profile, with a deviation of only  $\pm 2\%$ . Jin et al. [24] used PIV technology to investigate two-phase flow behavior with different media in pipelines. They found that PIV technology can improve measurement accuracy and characterize flow field flow characteristics more accurately. Wu et al. [25] conducted a visual experimental study on Taylor–Dean flow in a curved tube with a square section using PIV testing technology. Based on previous research, using PIV particle image velocity measurement technology is necessary to study the velocity change in the two-phase flow when the pig is running in a pipeline containing a liquid phase [26]. This paper employs PIV technology to investigate the relationship between the velocity variation in gas–liquid two-phase flow at different initial running velocities, liquid holdup, and liquid-phase volume fraction. Finally, the simulation results are compared and verified.



**Figure 1.** Pipeline corrosion morphology.

## 2. Research Methods

### 2.1. Experimental Planning and Working Condition

When utilizing PIV measurement technology for gas–liquid two-phase pipeline, the measurement of liquid-phase velocity is generally more straightforward than that of gas-phase velocity. Hence, this study initially calculates the liquid-phase velocity and subsequently determines the gas-phase velocity. An experimental platform was established to simulate pig-related tasks, as illustrated in Figure 1. The platform encompasses a pipeline, pig, a PIV measuring system, a servo motor, and other components. The PIV measuring system consists of a digital camera image system, a double-pulse laser system, synchronization controller, and other essential elements. Table 1 presents the key parameters. The schematic diagram of the PIV test is illustrated in Figure 2. The operational principle of this apparatus involves dispersing tracer particles with a specific density uniformly into the investigated flow field. A prism reflects the laser emitted by the lighting source, generating a sheet light that illuminates the target flow field. Subsequently, at least two exposures of

particle images are captured by a CCD camera. Finally, these particle images are processed and analyzed using a PIV image processing system to obtain an approximate instantaneous velocity profile of the flow field.

**Table 1.** Main parameters of the PIV test system.

Equipment Name	Equipment Parameter	Value
Digital camera image system	Minimum exposure interval	200 ns
	Collector resolution	3380 × 2710
	Grey levels	12 bit
Double-pulse laser system	Single pulse energy	500 MJ
	Wave length	532 nm
	Repetition frequency	1–10 HZ
	Pulse length	6–10 ns

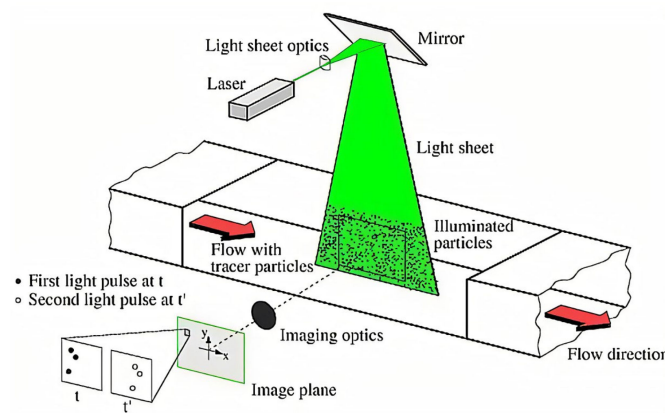


**Figure 2.** PIV schematic diagram.

To conduct the experiment, it is recommended to construct the platform illustrated in Figure 3. It is suggested that this experimental setup effectively simulates Reynolds numbers in pipelines under real working conditions, while taking into account the limitations of available experimental equipment. Following comprehensive field research, utilizing Formula (1), it has been determined that the Reynolds number in actual industrial production ranges from approximately 7000 to 15,000.

$$Re = \frac{\rho v D}{\mu} \tag{1}$$

$Re$  represents the Reynolds number,  $\rho$  represents the fluid density,  $v$  represents the fluid velocity away from the object,  $D$  represents the characteristic length, and  $\mu$  represents the dynamic viscosity coefficient.

Therefore, a 1.5 m pipe with a 50 mm inner diameter of plexiglass is selected to ensure sound-light transmission. Above the pipe is a water injection port that adds water through a funnel. Two liquid holds of 25% and 30% (the proportion of the liquid phase in the pipeline) were chosen for the pipeline. The initial running speed of the pig was adjusted to 0.3 m/s and 0.15 m/s, with ropes tied on both sides to drive the pig through the pipeline using an adjustable speed servo motor. According to the Reynolds number formula, the Reynolds numbers for the two pigging velocities are 7425.74 and 14,851.48, respectively. To ensure accuracy, both sides of the pipe were sealed with waterproof tape during experimentation. In this experiment, the front and back ends of the pipeline are sealed with waterproof adhesive to create a closed loop, aiming to enhance the accuracy of tracer particle addition and achieve a more realistic flow field velocity. However, during the experiment, some liquid impacts the sealant, resulting in reflux that affects the distribution of liquid velocity. After conducting multiple experiments, it was determined that the reflux

of the liquid phase occurring one meter away from the initial position of the pipeline has minimal impact on fluid velocity distribution. To accurately depict real-world conditions, a designated experimental test area was chosen at a distance of one meter from the initial position of the pipeline.

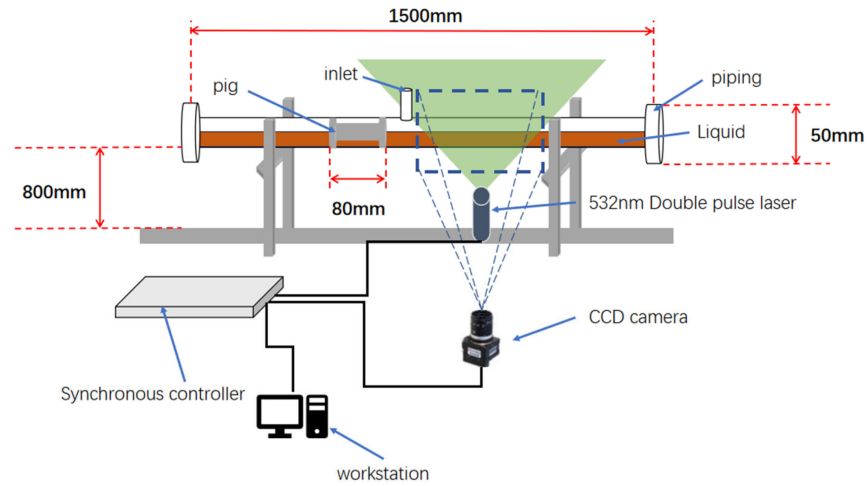


**Figure 3.** Schematic diagram of the experiment.

## 2.2. The Measurement Scheme

### 2.2.1. The Liquid-Phase Measurement Scheme

Due to the presence of a gas–liquid two-phase flow field in the test section, turbulence occurs during pig operation in the pipeline. This turbulence can lead to potential damage to the camera when capturing reflections from the liquid surface while running laser experiments, posing a safety hazard. To mitigate this issue, fluorescent particles composed of Rhodamine b are employed in the experiment. Rhodamine b exhibits excellent light transmission properties and exclusively reflects red light; therefore, a red filter is incorporated into the camera setup to eliminate liquid reflections. To verify the followability of the selected fluorescent particles, it is necessary to study their fluid mechanics characteristics. The Stokes number for Rhodamine b can be calculated using Equation (2). The characteristic time  $t_0$  can be calculated using Equation (3). With the particle size of Rhodamine b being 7 microns, the density being 0.79 g per cubic centimeter, the viscosity of the air being  $1.81 \times 10^{-5}$  kg (m·s), the velocity of the flow field away from the object being approximately 0.01 m/s, the Stokes number is obtained:  $0.84 \times 10^{-5}$ . When the Stokes number is much less than 0.1, the tracer accuracy error is 1%. It is verified that Rhodamine b has good followability. Stokes number can also prove the particle size in reverse.

$$Stk = \frac{t_0 u_0}{l_0} \tag{2}$$

$$t_0 = \frac{\rho_d d_d^2}{18 \mu_g} \tag{3}$$

The relaxation time of an object, represented by  $t_0$ , is related to the velocity of the flow field away from the object, represented by  $u_0$ , and the characteristic size of the object (generally diameter), represented by  $l_0$ . Meanwhile, the density of the object is represented by  $\rho_d$ , the viscosity of the gas by  $\mu_g$ , and the diameter of the object by  $d_d$ .

To introduce the fluorescent particles into the pipeline, they are premixed with bottled water and poured through a funnel into the opening above the pipe. The pig is then moved laterally to ensure uniform distribution of particles. For optimal dispersion of Rhodamine B in water, it is recommended to add only a few drops of Rhodamine B to each mixing session with bottled water. After vigorously shaking the bottle, sunlight should not penetrate through the liquid for achieving optimum mixing effect. In each injection cycle, 3–5 mL of

mixed Rhodamine B solution was added through the water injection port. The captured frames were repeatedly examined using a camera. The desired scattering density was achieved when fluorescent particles were uniformly distributed and clearly visible within the measured flow field. The camera should be positioned 50–100 cm away from the object to be measured, and the shooting area should be up to  $600 \times 800$  mm. The double-pulse laser should be placed at least 60 cm from the pipe, with its thinnest point at 0.5–1 mm, and aimed from the bottom up to avoid interference from external light sources. A black shading cloth should be used on the back side of the pipe to prevent such interference during the experiment.

### 2.2.2. Measurement Process

The experiment employed a waterproof adhesive to seal both sides of the pipeline instead of flanges, facilitating the operation of an adjustable speed servo motor for pig pulling and simulating pigging work. The pig was connected to a thin wire via the waterproof adhesive. This approach eliminated the need for flange drilling, simplifying installation and enabling precise control over pig speed, thereby achieving a more realistic flow field velocity. The primary objective of this experiment was to observe gas–liquid–phase velocity fluctuations during the pigging process in the pipeline. Figure 4 illustrates liquid holdup in the pipeline, Figure 5 shows the position of the pig in the pipe, while Figure 6 depicts the experimental test area captured, with specific test conditions detailed in Table 2.

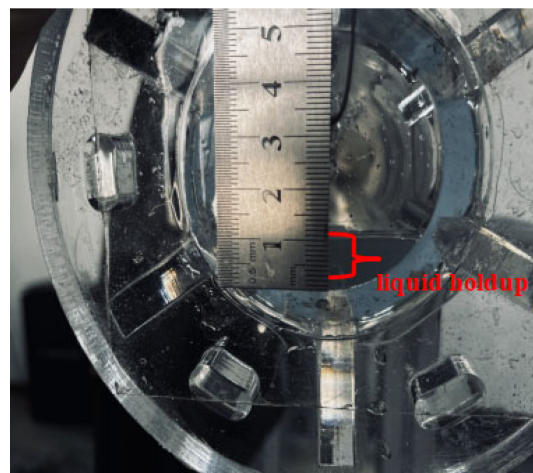


Figure 4. Liquid holdup.

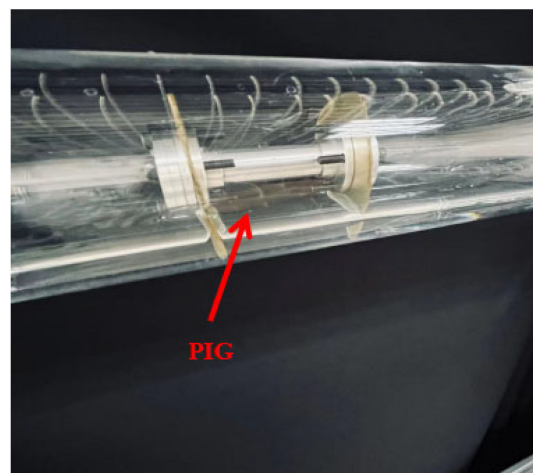


Figure 5. PIG.

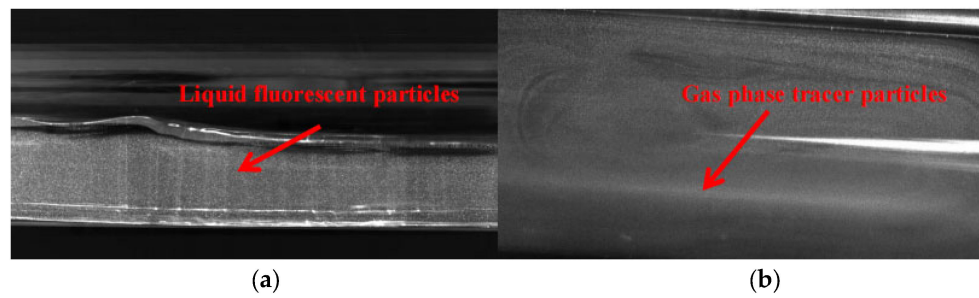


Figure 6. PIV shooting area. (a) Liquid-phase region; (b) gas-phase region.

Table 2. PIV liquid-phase test working condition.

Pig Speed	Liquid Holdup	Cross-Frame Time	Operating Frequency
m/s	mm	μs	HZ
0.3	30% 25%	1500	8
0.15	30% 25%	1000	8

### 2.2.3. The Gas-Phase Measurement Scheme

To conduct experiments in the gas phase, smoke particles measuring were chosen as labeled particles. As shown in Figure 7, these particles are generated and introduced into the pipe through spraying. To guarantee precise experimental results, it is essential to attach a green filter onto the camera (as demonstrated in Figure 8). Additionally, during the image capturing process above the liquid level, special attention should be given to adjusting CCD camera height carefully so as to avoid any damage caused by reflections resulting from fluctuations. All other procedures follow those used for liquid-phase measurements. A detailed description of the PIV spatial calibration and frame rate is essential to ensure accurate measurement space and relevance for practical applications during the PIV test. To better observe the velocity fluctuations of the gas–liquid two-phase, the laser frequency was set to 8 Hz, and the camera was adjusted to high-frequency mode, corresponding to a PIV frame rate of 16 fps. When the liquid holdup is 25% and the pigging speed is 0.3 m/s, the image magnification is 0.0828599 mm/pixel. Similarly, when the liquid holdup is 25% and the pigging speed is 0.15 m/s, the image magnification is 0.0578952 mm/pixel. Moreover, when the liquid holdup is 30% and the pigging speed is 0.3 m/s, the image magnification is 0.0373821 mm/pixel. Lastly, when the liquid holdup is 30% and the pigging speed is 0.15 m/s, the image magnification is 0.0407415 mm/pixel.



Figure 7. Particle generator.

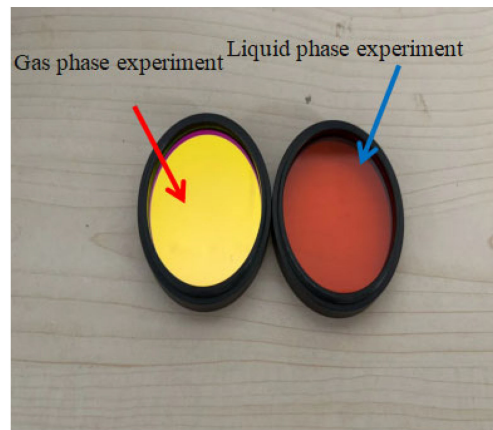


**Figure 8.** Filter.

### 2.3. Simulation Model Settings

To ensure the accuracy of the experimental results, it is imperative to compare them with those obtained from a Particle Image Velocimetry (PIV) test. This study employed Fluent, a reputable computational fluid mechanics tool, for conducting numerical simulations. To ensure the congruity between the simulation model and the pig utilized in the experiment, the conventional pig model selected which depicted in Figure 9. The dimensions chosen model are presented in Table 3.

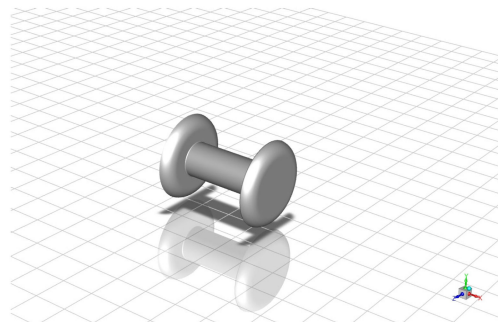


**Figure 9.** Pig model.

**Table 3.** PIG model and pipeline structure.

Name	Model Size
PIG	Length: 70 mm Cup diameter: 48 mm
Pipeline	Length: 1.5 m Inner diameter: 50 mm

The ICEM software (the version number is 2020 R2) was used to mesh the model. Due to the pig’s movement within the pipeline, conventional moving grid division methods fail to achieve convergence in calculating the gap between the pig and pipe wall. Implementing a moving grid division exacerbates this issue, resulting in poor simulation of the gap and non-convergence of results. To address this challenge, this study employs a grid nesting approach for division: one grid represents the pipeline while another encompasses the pig and its surrounding flow field. The zone motion model in Fluent software (the version number is 2020 R2) is adopted to facilitate control over pig movement within the pipeline. Initially, the pig is meshed, and a specific range of fluid areas outside it is selected. To ensure accurate calculation, it is necessary to encrypt the grid close to the wall. Subsequently, the pipeline is meshed, and similarly, to guarantee precise results and convergence in

calculations, the grid adjacent to the tube wall should be refined. The hexahedral structured grid was employed to subdivide and enhance the quality and accuracy of the analysis, thereby improving the overall precision. Subsequently, the subdivided pipeline robot mesh is nested within the pipeline mesh for further refinement. Figures 10 and 11 visually depict the segmentation of both the pipeline and pig, as well as provide an overview of the entire grid.

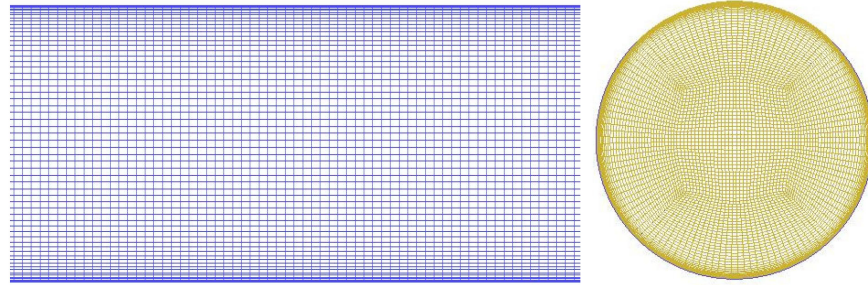


Figure 10. Pipeline mesh.

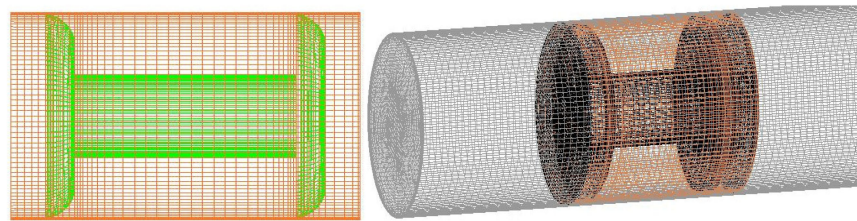


Figure 11. PIG and overall mesh.

In the simulation setup, the gas and liquid-phase velocities at the inlet are set to zero, which is consistent with the experimental findings. The volume fraction of liquid reflux through the pressure outlet is determined to be unity. Both the pig’s running speed and initial liquid-phase height align well with those observed in the experiment.

#### 2.4. Control Differential Equations and Turbulence Models

The pig model’s gravity problem is not taken into account during its establishment. Water is the medium used, which is a Newtonian incompressible fluid that satisfies Newton’s law of internal friction. The temperature change during pig operation is not considered due to the short set pipe length. The VOF model, which can predict the water–air interface, is chosen as the shape of the water–air interface needs to be observed. The QTH phase has a continuous phase equation:

$$\frac{1}{\rho_q} \left[ \frac{\partial}{\partial t} (a_q \rho_q) + \nabla \bullet (a_q \rho_q \vec{v}_q) \right] = S_{a_q} + \sum_{p=1}^n \dot{m}_{pq} - \dot{m}_{qp} \quad (4)$$

During the setup of the simulation, it was observed that the gas-phase and liquid-phase velocity at the inlet were both zero, which matched the expected values from the experiment. The volume fraction of liquid reflux was found to be one using the pressure outlet. The running speed of the pig and the initial height of the liquid phase were also consistent with the experiment. The pressure transient solver was selected as the solver for the simulation, while the k-ε model was chosen as the turbulence model. The turbulent kinetic energy k transport equation for the k-ε model is as follows:

$$\frac{\partial(\rho k)}{\partial t} + \frac{\partial(\rho k v_i)}{\partial x_i} = \frac{\partial}{\partial x_i} \left[ \left( \mu + \frac{\mu_t}{\sigma_k} \right) \frac{\partial k}{\partial x_i} \right] + G_k + G_b - \rho \epsilon - Y_M + S_\Phi \quad (5)$$

where  $G_k$  is the turbulent flow energy generated by the velocity gradient,  $G_b$  is the turbulent flow energy produced by buoyancy,  $\rho\varepsilon$  is the dissipate term,  $Y_M$  is a compressible correction item, and  $S_\phi$  is a custom source item. For incompressible fluids, without considering the buoyancy problem,  $G_b$ ,  $Y_M$ , and  $S_\phi$  are all 0.

The transport equation of the dissipation rate  $\varepsilon$  is:

$$\frac{\partial(\rho\varepsilon)}{\partial t} + \frac{\partial(\rho\varepsilon v_i)}{\partial x_i} = \frac{\partial}{\partial x_i} \left[ \left( \mu + \frac{\mu_t}{\sigma_\varepsilon} \right) \frac{\partial \varepsilon}{\partial x_i} \right] + \frac{G_{1\varepsilon}\varepsilon(G_K + C_{3\varepsilon}G_b)}{k} - \frac{C_{2\varepsilon}\rho\varepsilon^2}{K} + S_\Phi \quad (6)$$

where  $\frac{G_{1\varepsilon}\varepsilon G_k}{k}$  is a production item,  $\frac{G_{1\varepsilon}\varepsilon C_{3\varepsilon} G_b}{k}$  is the buoyancy correction term, and  $\frac{C_{2\varepsilon}\rho\varepsilon^2}{k}$  is the dissipative term.

### 2.5. The Gas–Liquid Two-Phase Flow Model

During the pigging process, the pipeline undergoes a gas–liquid two-phase flow. This two-phase flow can be categorized into six types: bubble flow, plug flow, stratified flow, wavy flow, slug flow, and annular flow. Among these types, stratified and wavy flows are commonly observed through experimental investigations. The present study illustrates the schematic diagram of wavy flow based on the developed pigging experiment platform as depicted in Figure 12. Within the pipeline system, it is imperative for the liquid phase to satisfy three fundamental equations:

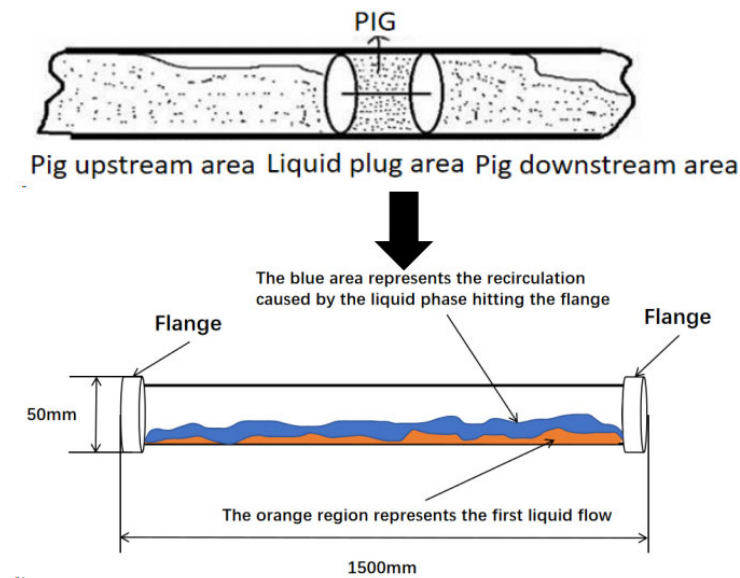


Figure 12. The wavy flow formed by the pigging process.

Mass conservation equation:

$$\frac{\partial \rho}{\partial t} + \frac{\partial(\rho u)}{\partial x} + \frac{\partial(\rho v)}{\partial y} + \frac{\partial(\rho w)}{\partial z} = 0 \quad (7)$$

Momentum conservation equation:

$$\frac{\partial}{\partial t}(\rho u_i) + \frac{\partial}{\partial x_j}(\rho u_i u_j) = -\frac{\partial \rho}{\partial x_j} + \frac{\partial \tau_{ij}}{\partial x_j} + \rho g_i + F_i \quad (8)$$

Energy conservation equation:

$$\frac{\partial}{\partial t}(\rho E) + \frac{\partial}{\partial x_i}(u_i(\rho E + p)) = \frac{\partial}{\partial x_i} \left( k_{eff} \frac{\partial T}{\partial x_i} - \sum_j h_j J_j + u_j(\tau_{ij})_{eff} \right) + S_h \quad (9)$$

### 3. Results and Discussion

#### 3.1. Liquid-Phase Velocity Analysis

After analyzing the PIV liquid-phase test results, two significant changes were observed in the shooting area. Initially, there was an accumulation of the liquid phase, followed by a period of stable distribution. Figure 13 presents the velocity cloud map derived from the PIV test results, providing a clearer visualization of the temporal evolution of liquid-phase velocities. During the calculation of the PIV vector, it was found that the interpretation area and step size are set to 64 and 32, respectively, which can better reflect the characteristics of the experimental flow field.

After analyzing cloud images, it was discovered that the velocity of the liquid phase exhibits rapid fluctuations. The time corresponding to each velocity change in the liquid surface was determined by employing an 8 Hz laser frequency and calculating it based on the total number of photos captured. As the initial operating speed of the pig increases, so does the velocity of its fluid phase; this acceleration in speed also intensifies with operational speed until a uniform liquid-phase velocity is attained throughout our testing area. All variations in fluid phase velocity manifest as appearing at the leftmost point and over time, there will be a gradual increment in liquid-phase velocity from left to right along our pipeline. The subsequent analysis will concentrate on two specific instances where changes in liquid-phase velocity were observed within our shooting area.

This analysis examines the initial velocity of the liquid phase generated during pig operation. During the experiment, two different fluid holdup rates were selected. The corresponding liquid-phase distribution and velocity vector images are depicted in Figures 14 and 15, respectively. Upon examining the velocity vector diagram, it is evident that the velocity direction aligns with the pig’s running direction, from left to right. The region exhibiting concentrated velocity direction coincides with the initial deposition site of the liquid phase. Furthermore, higher velocities can be observed in the liquid phase near the water–gas interface compared to other positions. To accurately capture variations in liquid-phase velocity, a data extraction line measuring 25 mm along the Y direction was selected as indicated by the red dotted line.

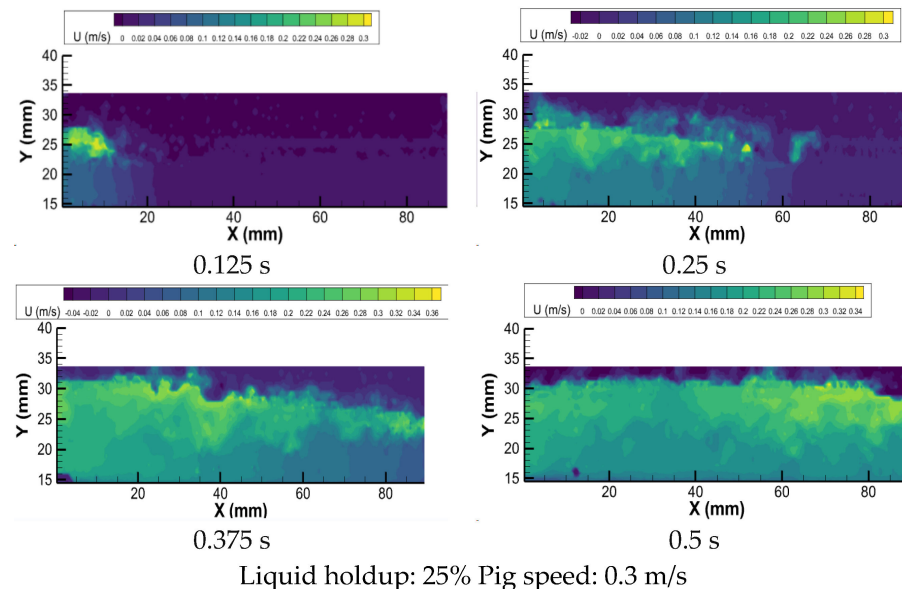


Figure 13. Cont.

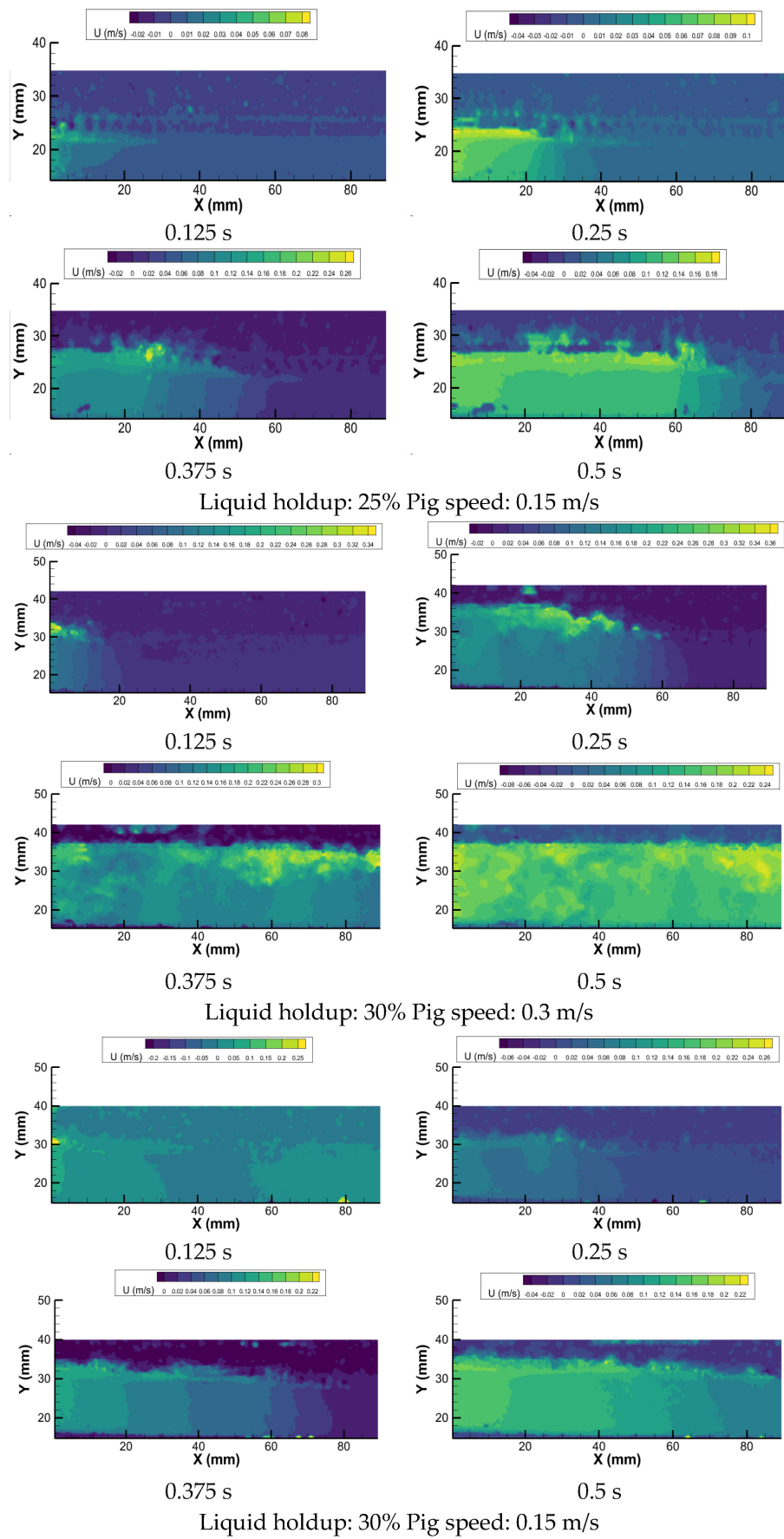


Figure 13. PIV velocity cloud (liquid phase).

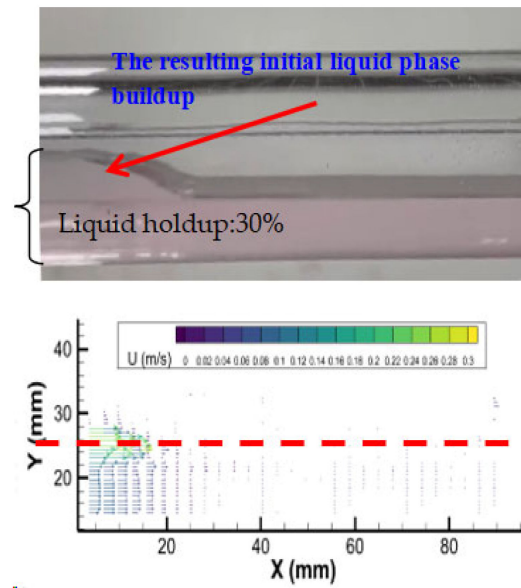


Figure 14. Initial liquid-phase buildup (30%).

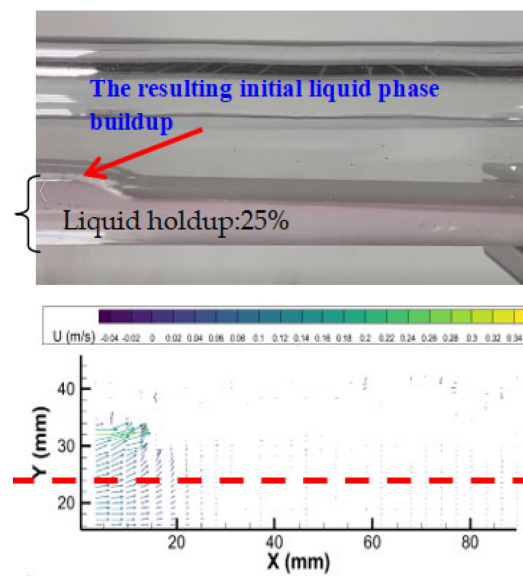
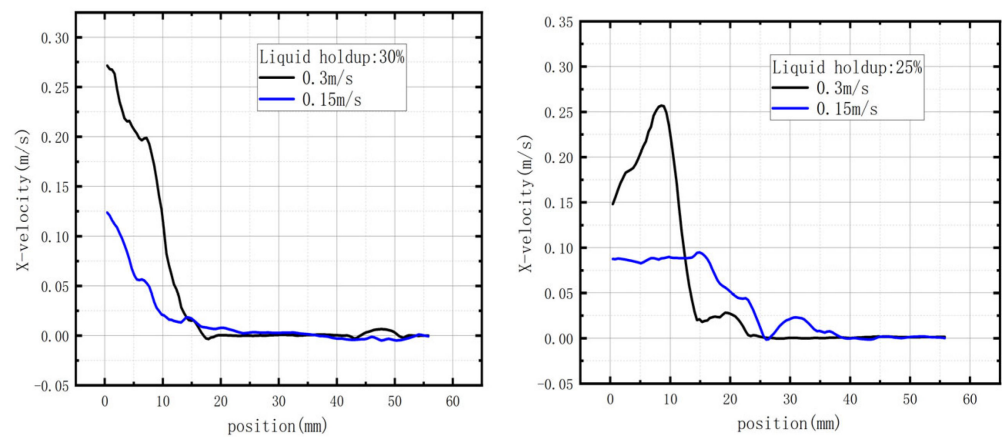


Figure 15. Initial liquid-phase buildup (25%).

Figure 16 shows the change of liquid velocity at each point with initial liquid deposition. Upon analyzing the velocity variation in the initial liquid-phase deposition, it becomes evident that the velocity peaks initially and then gradually decreases to zero as the initial operating speed of the pig increases. The velocity fluctuation of the liquid phase gradually increases as well. An increase in the initial height of the liquid surface also leads to an increase in the fluctuation of the fluid phase velocity. However, the maximum liquid-phase speed does not exceed the initial operating speed of the pig. At 30% holdup, the ultimate liquid-phase velocity is 10% lower than the initial operating speed of the pig.



**Figure 16.** Velocity change in the liquid phase in the X direction (Initial liquid phase accumulation).

Similarly, at a holdup of 25%, the maximum liquid-phase velocity is 16% lower than the initial operating velocity of the pig. The velocity of the liquid phase is directly related to the volume fraction of the liquid phase at the initial liquid-phase deposition. The fluid velocity is higher where there is liquid deposition and zero where there is no liquid deposition. Since the liquid-phase velocity is directly proportional to the dynamic pressure of the pig, it is recommended to install a guide plate at the front end of the pig during the design process to enhance its working life [27].

The diagram below illustrates the velocity of the liquid phase during its transition to a stationary state. Figures 17 and 18 depict the distribution of the fluid phase at different liquid level heights and the corresponding vector representing the velocity of the liquid phase, as observed in our experimental study. Our findings indicate that there is a consistent left-to-right movement of the liquid phase, aligning with the direction of flow indicated by the pig’s motion. Additionally, it should be noted that for data collection purposes, our extraction line was positioned at a distance of 25 mm along the Y-axis, as shown by the red dotted line.

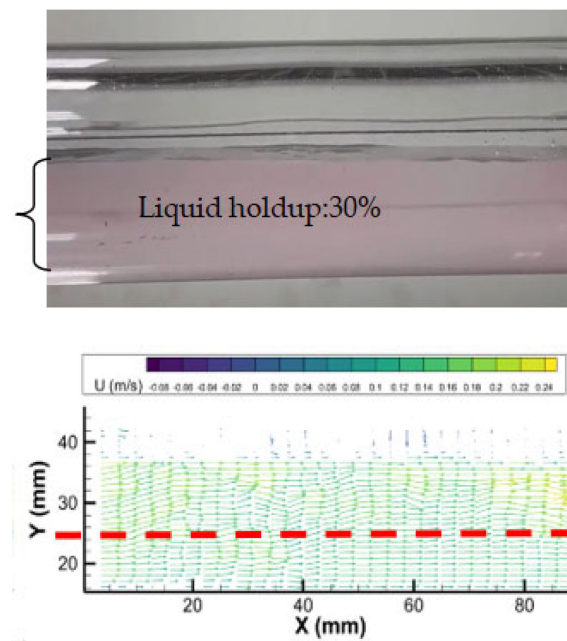


**Figure 17.** Liquid-phase stationary state (30%).

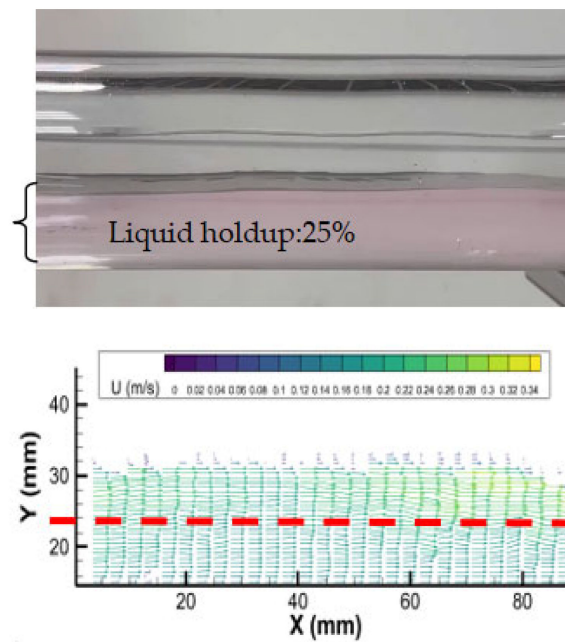


Figure 18. Liquid-phase stationary state (25%).

Based on the PIV test results, it is evident that the speed of the liquid phase during the stationary period varies at different points. When observing the fluid phase velocity in the direction of Figure 19. X, it initially decreased and then increased. Once raised the pigging speed to 0.3 m/s, there was a significant change in the liquid-phase velocity. The fluctuation amplitude of fluid velocity increases with the increase in the initial liquid level. However, the range of fluctuation of liquid-phase velocity did not exceed the initial operating speed of the pig, and the difference between the minimum speed and the maximum speed was within 0.1 m/s. The change in the liquid-phase velocity in the pipeline is more drastic when the initial operating speed of the pig is more significant. Therefore, the front end of the pig cup has greater fatigue strength than the back end. Based on the experimental results presented above, it can be inferred that a higher pigging speed has a more significant impact on the front end of the pig bowl. Therefore, when a pigging operation requires increased pigging speed, replacing the front-end leather bowl with better fatigue resistance is advisable. This will help to enhance pigging efficiency. It is important to note that the above research is based on a specific time, and the liquid-phase velocity changes at each location photographed were observed. To increase the persuasiveness of the conclusion, the transient changes in fluid phase velocity was further analyzed.

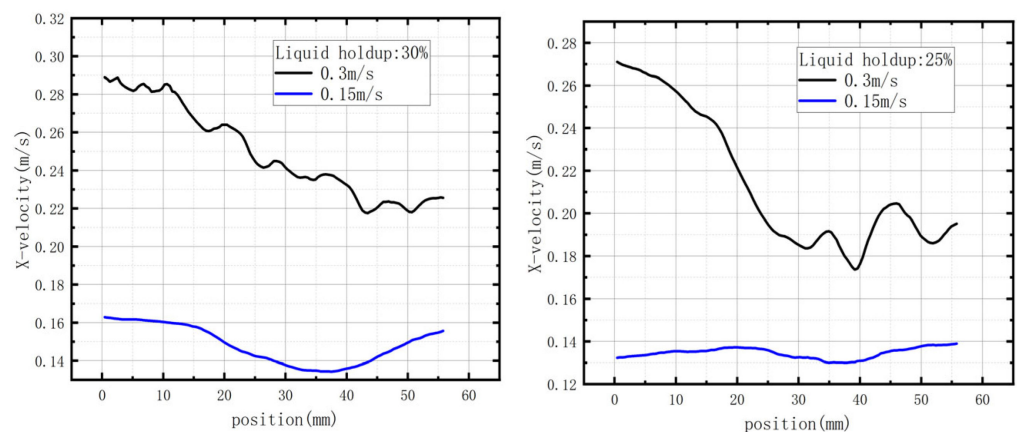


Figure 19. Velocity change in the liquid phase in the X direction (Liquid-phase stationary state).

The experiment was repeated three times for each condition. A data extraction point of 20 mm in the X direction was selected to observe the liquid phase’s velocity directly. The analysis quantitatively examined the variation in fluid velocity at different heights. As shown in Figure 20, when the liquid holdup is 25%, the liquid-phase velocity gradually increases over time. The period between 0.125 and 0.375 s is the liquid-phase accumulation and migration process, in which the liquid-phase velocity rises the most. After 0.375 s, the fluid phase velocity becomes stable. On average, for every 5 mm increase in the Y direction, the liquid-phase velocity increases by 20%. When the holdup rate is 30%, it is observed that the liquid-phase velocity increases steadily with time. Compared to the liquid holdup of 25%, the fluid velocity at different heights tends to be the same. Therefore, it is concluded that the liquid velocity becomes uniform to varying heights as the liquid holdup increases. Once the accumulation and migration of the liquid phase is complete, the velocity of the liquid phase becomes stable. When the amount of liquid in the pipeline is less than 25%, the speed of the fluid flowing through the pipeline is higher near the top of the liquid level. During the pigging process, the center of the inner wall of the pipeline is more susceptible to corrosion than the bottom of the inner wall. Therefore, a coating or spray is applied to the central area of the inner wall of the pipeline to improve its corrosion resistance. This finding is helpful for the maintenance of natural gas pipelines.

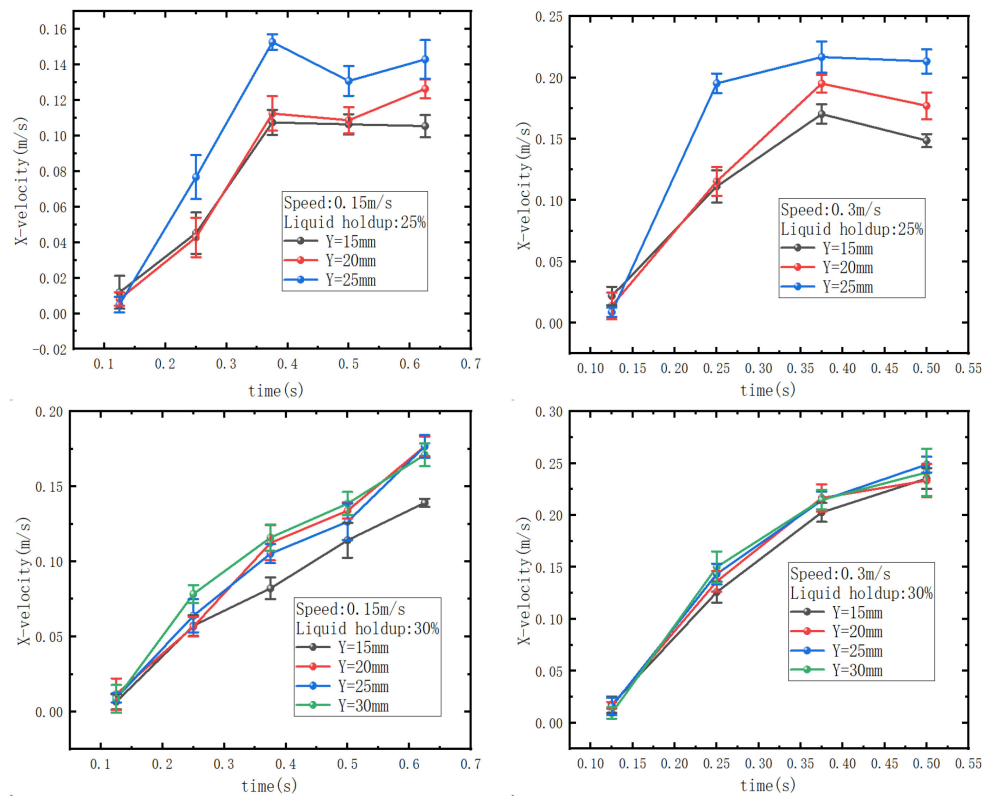
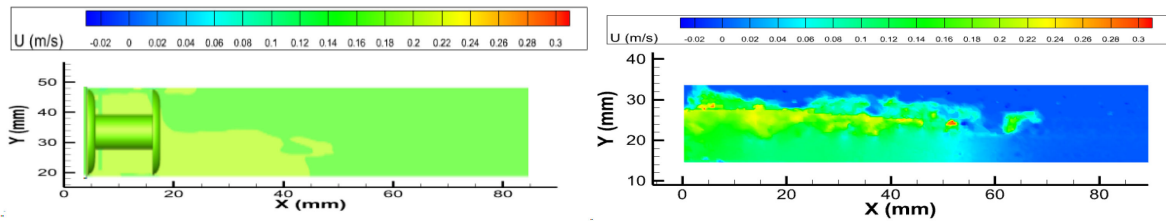


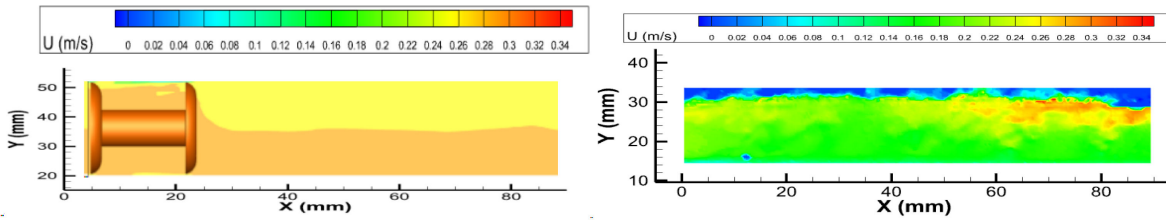
Figure 20. Transient changes in liquid-phase velocity and error bar.

### 3.2. Comparative Analysis of Simulation Results

The simulation was utilized for comparison and verification to demonstrate the accuracy of the experimental findings. Initially, the liquid-phase velocity obtained through simulation was compared with the velocity acquired from the PIV test. Figure 21 presents the simulated cloud image depicting the velocity distribution of the liquid phase and the corresponding cloud image acquired during the experimental investigation.

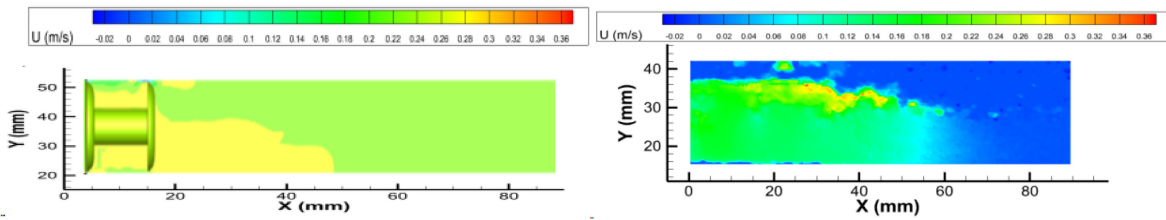


State 1: There is initial liquid-phase accumulation at the liquid surface.

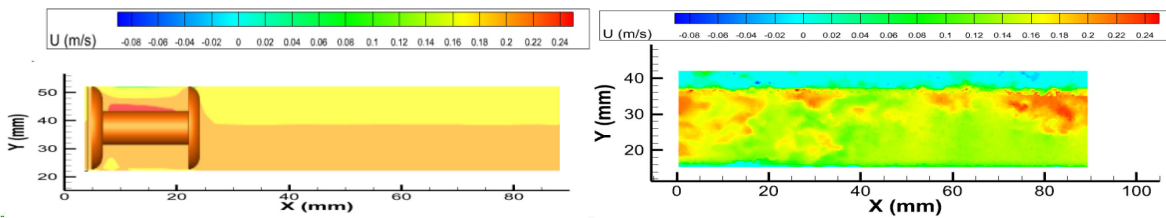


State 2: The liquid level is stable.

Initial operating speed of pig: 0.3 m/s liquid holdup: 25%



State 1: There is initial liquid-phase accumulation at the liquid surface.



State 2: The liquid level is stable.

Initial operating speed of pig: 0.3 m/s liquid holdup: 30%

Figure 21. Liquid-phase velocity cloud.

The left side displays a simulation-derived image of liquid velocity, while the right side presents an image of fluid velocity obtained through PIV testing. The simulation results demonstrate that the liquid-phase velocity corresponds to the experimental findings when an initial accumulation of the liquid phase occurs. A specific liquid-phase velocity is associated with accumulation, whereas no accumulation leads to zero velocity. Despite potential external factors such as distortion caused by the circular wall of the pipeline during camera capture, the experimental results align well with those obtained from simulations. Figure 22 illustrates a comparison between these two sets of results, and subsequently, this study analyzes variations in the volume fraction of the liquid phase.

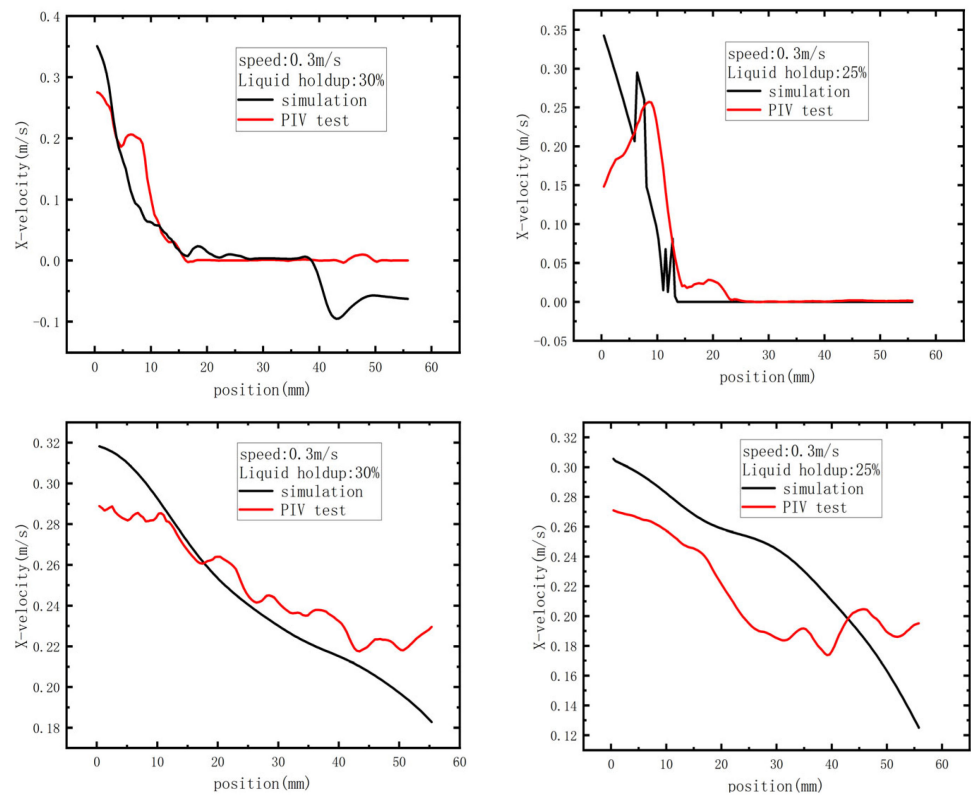


Figure 22. Comparison of PIV test results with simulation.

Error Analysis

To enhance the accuracy of the experimental findings, the initial operating speed of the pig has been set to 0.3 m/s, as this speed change is more noticeable. This serves as a qualitative verification, considering that the observed speed of the pig is 0.3 m/s. Table 4 presents the absolute error of the numerical simulation and PIV experiment results.

Table 4. Experimental error of liquid-phase velocity numerical simulation and PIV measurement results.

(a) Initial liquid-phase buildup			
Initial pig operating speed	0.3 m/s		
Liquid holdup in the pipeline	25%	30%	
Mean absolute error	51.54%	57.04%	
(b) When the surface is in a steady state			
Initial pig operating speed	0.3 m/s		
Liquid holdup in the pipeline	25%	30%	
Mean absolute error	17.45%	6.31%	

Based on a comparison of errors, it is evident that the error becomes more significant in the presence of an initial accumulation of the liquid phase. This can be attributed to a pronounced variation in velocity range and distortion of the photographed particles caused by the curved tube wall during experimentation, resulting in a discernible level of specific error.

In Figure 23, the values of 0.3 and 0.15 denote the initial velocity of the pig, while 25% and 30% represent the pipeline’s initial liquid volume. Upon examining the figure, it is evident that as the pig’s starting speed increases, there is a more pronounced accumulation of liquid in the pipeline. Moreover, when there is a higher initial liquid level in the pipeline, there is a more conspicuous buildup of the liquid phase.

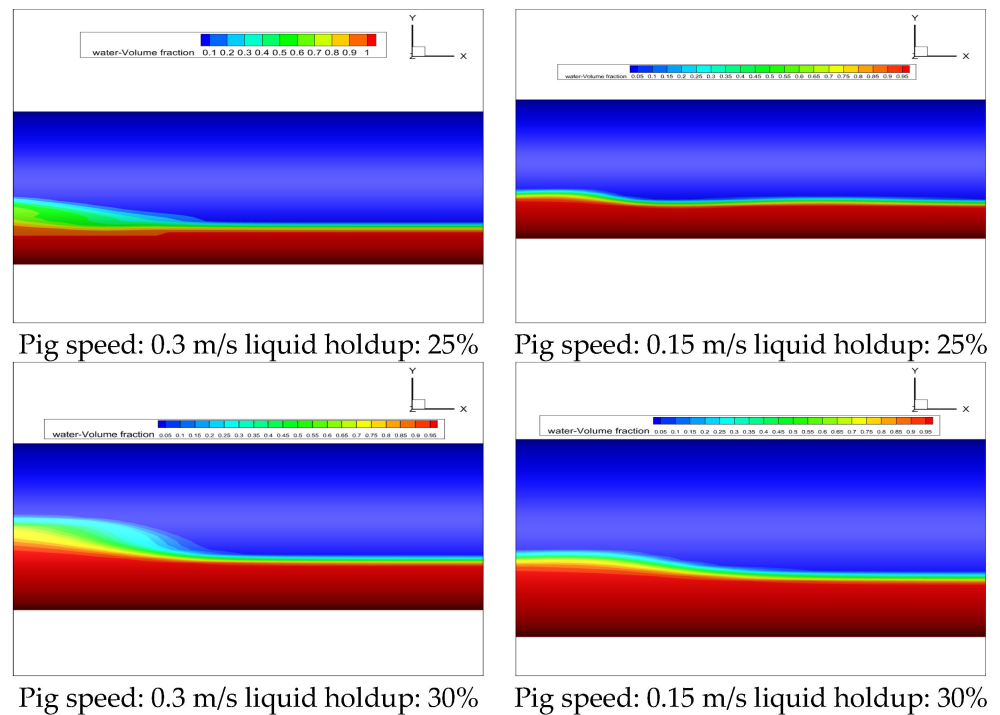


Figure 23. Comparison of liquid-phase volume fractions.

By simulating the volume fraction of the liquid phase, it can be observed that it follows a trend similar to that of the liquid-phase velocity, gradually decreasing in size. As shown in Figure 24. Initially, the volume fraction of the liquid phase is close to 1 and then slowly drops to zero. Adjusting the initial height of the liquid level results in an amplified trend as the initial liquid level increases. Moreover, elevating the pig’s initial operating speed leads to a reduction in the volume fraction of the liquid phase. This confirms that changes in the fluid volume fraction within the pipeline are directly proportional to changes in the liquid velocity within the pipeline.

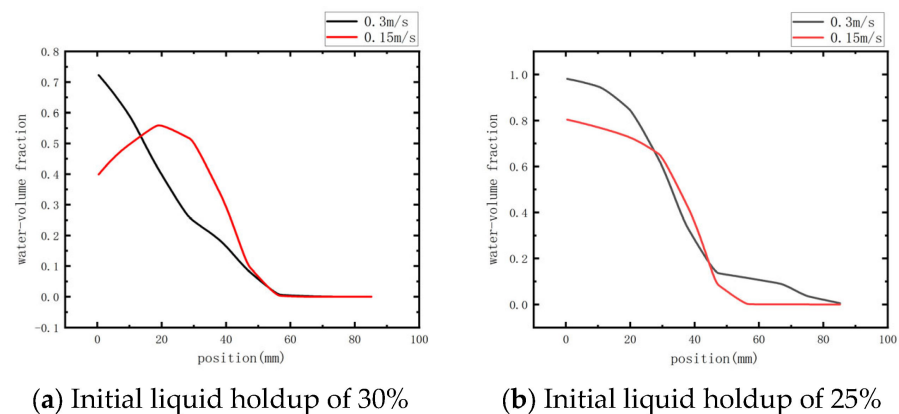


Figure 24. Liquid-phase volume fraction at initial liquid-phase deposition.

### 3.3. Gas-Phase Velocity Analysis

It is currently unclear how the initial operating speeds of a pig and the gas-phase velocity in a pipeline are related. This makes it challenging to choose an appropriate approach to plug the pig [28,29]. Examining the changes in gas-phase velocity within the pipeline is essential to gain more clarity. Our analysis focuses on the velocity patterns of the gas phase under conditions consistent with the liquid phase. Figure 25 shows the gas phase velocity vector diagram. Experimental results indicate that the velocity changes in the gas

phase do not mirror the structural changes in the liquid phase. Thus, the gas-phase average velocity trends across different working conditions can be explored. The gas-phase velocity test involves using carbon dioxide as the primary material for tracer particles. However, compared to the liquid-phase test, the tracking performance of these particles is weaker. Additionally, when the motor pulls the pig, the gas-phase tracer particles diffuse more quickly, which may somewhat affect the gas-phase velocity distribution.

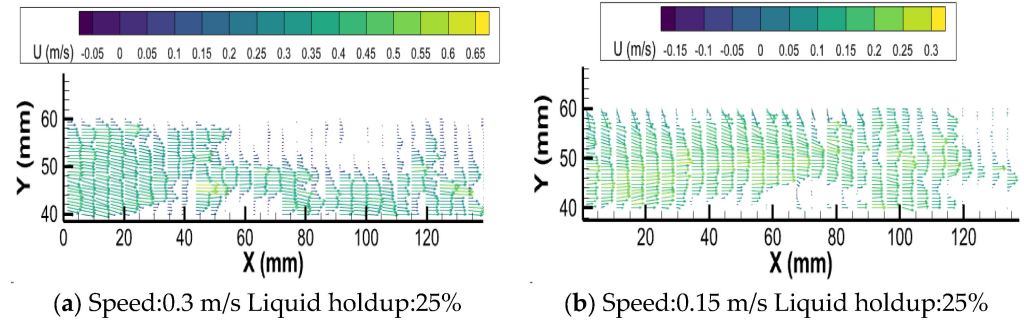


Figure 25. Gas-phase velocity vector diagram.

The obtained gas phase velocity changes are shown in Figure 26. Experimental results from the gas phase show a significant decrease in the gas-phase velocity after 80 mm in the X direction, which differs from the velocity change observed in the liquid phase. The change in gas-phase velocity is greatly affected by the liquid holdup. When the liquid holdup is 25%, the gas-phase velocity changes significantly, while at 30% holdup, the change is relatively stable. The gas-phase velocity change range is more significant at lower liquid holdup. It is observed that the maximum gas-phase velocity under different working conditions is larger than the initial operating speed of the pig, and the increase is not more than 0.1 m/s. The maximum average gas-phase velocity increased by 33.3% compared with pigging velocity. Therefore, when the pig is plugged, the plugging speed should be slightly more significant than the initial operating speed to provide a plugging plan.

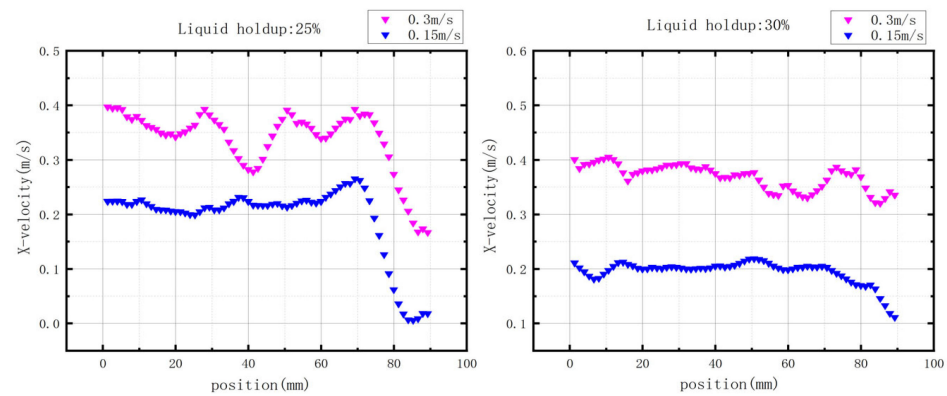
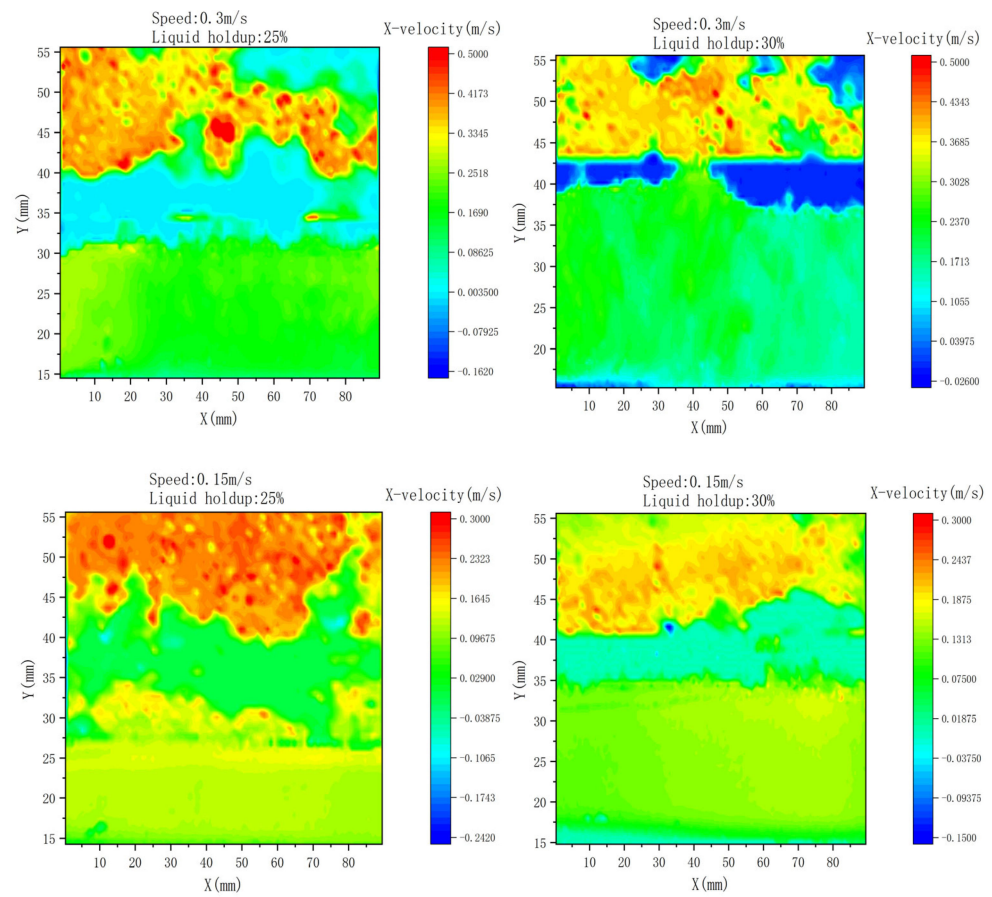


Figure 26. Gas-phase velocity changes under different working conditions.

### 3.4. Gas–Liquid Two-Phase Velocity Analysis

This analysis examines the changes in velocity for both the liquid and gas phases in a pipeline. To better understand how the velocity changes for both phases, their respective velocities were imported into the same image using image processing technology. As shown in Figure 27. The resulting velocity cloud image shows the velocity changes for both phases under different working conditions. The image indicates that the liquid phase is stable when the velocity is below 40 mm in the Y direction, while velocities above 40 mm belong to the gas phase.



**Figure 27.** Gas–liquid two-phase velocity cloud.

After comparing gas–liquid two-phase velocity cloud images across four different working conditions, it becomes clear that the gas-phase velocity in the pipeline is greater than the liquid-phase velocity, regardless of the conditions. Additionally, when the liquid holdup in the pipeline is increased while maintaining the initial speed of the pig, the gas-phase velocity decreases. When comparing the flow field structures of the gas and liquid phases, it is evident that the gas phase has an irregular form while the liquid phase presents a consistent distribution that correlates with the volume of liquid in the pipeline. The liquid height increases as the liquid holdup increases, but the fluid velocity remains relatively constant. The specific value of the gas–liquid two-phase velocity depends on the initial running speed of the pig. The liquid-phase speed should be lower than the initial operating speed of the pig, and the gas-phase velocity should be more significant. The difference between the maximum gas-phase velocity and its operating speed should not exceed 0.2 m/s. At the interface between the gas and liquid phases, the velocity is close to zero due to tracer particles blocked by the pipeline when the pig is in motion. To ensure the pig’s efficiency in a gas–liquid two-phase pipeline, it is important to consider improving its gas-phase corrosion resistance [30].

#### 4. Conclusions

This study investigates the variation in the velocity of gas and liquid phases as a pig traverses through a pipeline containing both phases. By employing Particle Image Velocimetry (PIV) measurement, image processing techniques, and numerical simulations, this research examines the characteristics of velocity variation in gas–liquid-phase flow within the pipeline. Specifically, this study focuses on exploring how the initial liquid content and operating speed of the pig influence changes in two-phase velocities. Furthermore, it analyzes variations in liquid-phase volume fraction and compares lateral velocity differ-

ences between the gas and liquid phases. The key findings obtained from this investigation are as follows:

- (1) When the initial liquid holdup is fixed, the liquid-phase velocity generated in the pipeline increases with the more considerable running speed of the pig. At 30% holdup, the maximum liquid-phase velocity is 10% lower than the pig's initial operating speed. At 25% holdup, the ultimate liquid-phase velocity is 16% lower than the pig's initial operational velocity. However, the maximum liquid-phase velocity does not exceed the initial operating velocity of the corresponding pig. Regarding liquid-phase height, the velocity increases on average by 20% for every 5 mm increase in the Y direction.
- (2) The proportion of the liquid content volume is directly related to the fluid velocity. As the initial liquid holdup and pig running speed increase, the liquid content volume fraction in the pipeline also increases gradually. However, the change in the fluid content volume fraction at the initial liquid deposit increases with the pig's rising liquid holdup rate and initial running speed. Therefore, during the pigging operation, it is necessary to consider the fluid holdup rate and the initial running speed of the pig and install a deflector to increase the pig's working life and improve pigging efficiency.
- (3) When using a pig to clean a pipeline, it is essential to remember that the pig's speed affects the gas flow velocity in the pipeline. As the pig moves faster, the gas flow velocity increases. It is important to note that the maximum gas flow velocity will be greater than the initial operating speed of the pig. The maximum average gas flow velocity can be up to 33.3% higher than the pigging velocity. Therefore, when plugging the pig, it is necessary to consider that the plugging speed is greater than the initial operating speed of the pig to provide a scheme for promoting the pig.
- (4) The gas-phase velocity cloud map indicates that the change in the gas phase is more noticeable than that of liquid-phase velocity. By comparing the gas–liquid-phase velocity, it was found that the velocity of the liquid phase is lower, and its distribution is regular and even throughout the pipeline. On the other hand, the gas-phase velocity distribution is irregular and decreases with the increase in initial liquid holdup. Therefore, when the liquid holdup in the pipeline is low, it is essential to focus on improving the corrosion resistance of the pig to the gas phase. This study explicitly investigated the gas–liquid two-phase flow in a pipeline. However, to enhance understanding of the pigging process under such conditions, it is crucial to measure velocity changes at the gas–liquid interface within the pipeline. Therefore, further research is warranted through conducting a comprehensive investigation on gas–liquid two-phase synchronous testing.

**Author Contributions:** Conceptualization, Y.Z. and S.C.; methodology, Y.Z.; software, Y.Z.; validation, Y.Z., S.C. and T.S.; formal analysis, Y.Z.; investigation, Y.Z.; resources, S.C.; data curation, S.C.; writing—original draft preparation, Y.Z.; writing—review and editing, S.C.; visualization, S.C.; supervision, S.C.; project administration, Y.Z.; funding acquisition, S.C. and Y.G. All authors have read and agreed to the published version of the manuscript.

**Funding:** This work was supported by the National Natural Science Foundation of China (U1908228).

**Institutional Review Board Statement:** Not applicable.

**Informed Consent Statement:** Not applicable.

**Data Availability Statement:** The data presented in this study are available on request from the corresponding author. The data are not publicly available due to scientific needs.

**Conflicts of Interest:** The authors declare no conflict of interest.

## References

1. Shan, H.; Zhu, Y.; Lang, X.A. Small Leak Detection and Localization Method for Oil Pipelines Based on Improved Robust Principle Component Analysis. *J. Phys. Conf. Ser.* **2022**, *2264*, 12021. [\[CrossRef\]](#)
2. Hu, J.; Tao, T. Numerical investigation of ice pigging isothermal flow in water-supply pipelines cleaning. *Chem. Eng. Res. Des.* **2022**, *182*, 428–437. [\[CrossRef\]](#)
3. Luo, H.; Meng, C.; Li, C. Design of a remote-controllable pipeline inspection robot with a robotic arm. In Proceedings of the Seventh International Conference on Electromechanical Control Technology and Transportation, Guangzhou, China, 23 November 2022; Volume 12302.
4. Hudaya, Z.A.; Widyatama, A.; Dinaryanto, O. The liquid wave characteristics during the transportation of air-water stratified co-current two-phase flow in a horizontal pipe. *Exp. Therm. Fluid Sci.* **2019**, *103*, 304–317. [\[CrossRef\]](#)
5. Figueiredo, B.A.; Baptista, M.R.; de Freitas Rachid, F.B.; Bodstein, G.C.R. Numerical simulation of stratified-pattern two-phase flow in gas pipelines using a two-fluid model. *Int. J. Multiph. Flow* **2017**, *88*, 8830–8849. [\[CrossRef\]](#)
6. Xu, X.; Gong, J. Pigging simulation for horizontal gas-condensate pipelines with low-liquid loading. *J. Pet. Sci. Eng.* **2005**, *48*, 272–280. [\[CrossRef\]](#)
7. Sadeghi, H.M.; Chitsaz, S.; Etefagh, M.M. Effect of PIG's physical parameters on dynamic behavior of above ground pipeline in pigging operation. *Mech. Syst. Signal Process* **2019**, *132*, 692–720. [\[CrossRef\]](#)
8. Wen, W.; Shi, M.; Shang, N.; Yin, L. Vibration Analysis for Pigging of Suspension Pipe Bridge. *Appl. Mech. Mater.* **2012**, *1968*, 669–672.
9. Liu, Y.; Zhu, X.; Song, J.; Wu, H.; Zhang, S.; Zhang, S. Research on bypass pigging in offshore riser system to mitigate severe slugging. *Ocean Eng.* **2022**, *246*, 110606. [\[CrossRef\]](#)
10. Deng, T.; Zhou, J.; Liang, G.; Xiao, Y.; Zhu, B.; Gong, J. Numerical Simulation of Pigging Operation through Curved Pipeline Coupling a T-Abort and Bend Drain Pipe. *J. Pipeline Syst. Eng. Pract.* **2021**, *12*, 04020052. [\[CrossRef\]](#)
11. Wang, W.; Huang, Q.; Liu, Y.; Sepehrnoori, K. Experimental study on mechanisms of wax removal during pipeline pigging. In Proceedings of the SPE Annual Technical Conference and Exhibition, Houston, TX, USA, 28–30 September 2015; SPE: Richardson, TX, USA, 2015; p. D021S019R004.
12. Nieckele, A.; Braga, A.; Azevedo, L. Transient Pig Motion Through Gas and Liquid Pipelines. *J. Energy Resour. Technol.* **2001**, *123*, 260–269. [\[CrossRef\]](#)
13. Mirshamsi, M.; Rafeeyan, M. Dynamic analysis and simulation of long pig in gas pipeline. *J. Nat. Gas Sci. Eng.* **2015**, *23*, 294–303. [\[CrossRef\]](#)
14. Sousa, A.; Pereira, M.J.; Matos, H.A. Planning pipeline pigging operations with predictivemaintenance. *E3S Web Conf. EDP Sci.* **2021**, *266*, 01017. [\[CrossRef\]](#)
15. Hendrix, M.H.W.; Ijsseldijk, H.P.; Breugem, W.P.; Henkes, R. Experiments and modeling of by-pass pigging under low-pressure conditions. *J. Process Control* **2018**, *71*, 1–13. [\[CrossRef\]](#)
16. Li, X.; He, L.; Luo, X.; Liu, H.; He, S.; Li, Q. Transient pigging dynamics in gas pipelines: Models, experiments, and simulations. *Ocean Eng.* **2021**, *232*, 109126. [\[CrossRef\]](#)
17. Jamshidi, B.; Sarkari, M. Simulation of pigging dynamics in gas-liquid two-phase flow pipelines. *J. Nat. Gas Sci. Eng.* **2016**, *32*, 407–414. [\[CrossRef\]](#)
18. Chen, J.; He, L.; Luo, X.; Zhang, H.; Li, X.; Liu, H.; He, S.; Lu, L. Characterization of bypass pig velocity in gas pipeline: An experimental and analytical study. *J. Nat. Gas Sci. Eng.* **2020**, *73*, 103059. [\[CrossRef\]](#)
19. Zhang, L.; Zhou, J.; He, H. Modeling and simulation of pigging for a gas pipeline using a bypass pig. *Math. Probl. Eng.* **2020**, *2020*, 1–12. [\[CrossRef\]](#)
20. Wu, X.; Niu, S.; Li, C. The study of the dynamic response of the natural gas pipeline aerial crossing during pigging process: A Review. *J. Fluids Struct.* **2021**, *105*, 103339. [\[CrossRef\]](#)
21. Hendrix, M.; Liang, X.; Breugem, W.; Henkes, R. Characterization of the pressure loss coefficient using a building block approach with application to by-pass pigs. *J. Pet. Sci. Eng.* **2016**, *150*, 13–21. [\[CrossRef\]](#)
22. Rao, P.; Yelgaonkar, V.N.; Tiwari, C.B.; Dhakar, V.; Panicker, M. Locating block caused by stuck PIGs in multi product pipeline using combination of radioisotope techniques. *Appl. Radiat. Isot.* **2023**, *193*, 110660. [\[CrossRef\]](#)
23. Zhang, Y.; Wang, J. Measurement of flow in rectangular micropipes by micro-PIV. *J. Exp. Fluid Mech.* **2011**, *25*, 92–95.
24. Jin, X.; Deng, Y.; Liu, G.; Chen, B. Research on pipeline flow characteristics based on PIV technology. *Appl. Chem. Ind.* **2020**, *49*, 430–434+438.
25. Wu, X.; Zao, S.; Yong, L. Measurement of flow in bent pipe based on PIV method. *Hydraul. Pneum.* **2014**, *06*, 39–42.
26. Cheng, W.; Murai, Y.; Sasaki, T.; Yamamoto, F. Bubble velocity measurement with a recursive cross correlation PIV technique. *Flow Meas. Instrum.* **2005**, *16*, 35–46. [\[CrossRef\]](#)
27. Wen, C.; Zheng, Y.; Mi, D.; Qian, Z.; Zhang, H. Design for the Vent Holes of Gas Turbine Flow Guide Disks Based on the Shape Optimization Method. *Metals* **2023**, *13*, 1151. [\[CrossRef\]](#)
28. Chen, J.; He, L.; Luo, X.; Lu, L.; Zhang, H.; Li, X.; Liu, H.; He, S. Bypass pigging technology on amelioration of pigging-induced liquid flow: An experimental and modelling study. *Ocean Eng.* **2020**, *198*, 106974. [\[CrossRef\]](#)

29. Teyssandiert, R.G.; Wilson, M.P. An analysis of flow through sudden enlargements in pipes. *J. Fluid Mech.* **1974**, *64*, 85–95. [[CrossRef](#)]
30. Wang, X.; Ghidaoui, M.S. Pipeline leak detection using the matched-field processing method. *J. Hydraul. Eng.* **2018**, *144*, 04018030. [[CrossRef](#)]

**Disclaimer/Publisher’s Note:** The statements, opinions and data contained in all publications are solely those of the individual author(s) and contributor(s) and not of MDPI and/or the editor(s). MDPI and/or the editor(s) disclaim responsibility for any injury to people or property resulting from any ideas, methods, instructions or products referred to in the content.